River Flow 2010 - Dittrich, Koll, Aberle & Geisenhainer (eds) - © 2010 Bundesanstalt für Wasserbau ISBN 978-3-939230-00-7

Retention of dye tracer in side basins exchanging with subcritical and supercritical flows

Tao Wang, Shooka Karimpour Ghannadi & Vincent H. Chu
Department of Civil Engineering, McGill University, Montreal, Quebec H3A 2K6, Canada

ABSTRACT: The transverse exchanges of mass between an open-channel main flow and an array of side basins were studied in the laboratory using dye as the tracer. A video imaging method was employed to measure the dye concentration. The accumulation and retention times of the dye in the side basins are determined as the parameters to characterize the exchanges. The energetic radiation of the gravity waves in the supercritical flow does not lead to vigorous exchanges. On the contrary, the dimensionless retention time for the supercritical flow at a high Froude number was three to four times greater than the retention time for the subcritical flow.

Keywords: Lateral exchanges, Shallow shear flow, Coherent eddies, Shocklets, Supercritical flow.

1 INTRODUCTION

The transverse exchanges of mass across the subcritical shear flows in rivers are relatively understood. Many previous experimental investigations have been conducted. Almost all are concerned with the subcritical flow. The study of the subcritical flow exchanges include the works of Alavian & Chu (1985), Tamai et al. (1986), Booij (1989), Knight & Shiono (1990), Lambert and Sellin (1996), Altai & Chu (1997), Uijttewaal and Booij (2000) and van Prooijen et al. (2005). Flow exchanges in subcritical flow are primarily due to the rollup of fluid by the turbulent eddies. On the other hand, the process in supercritical flow is different. The radiation and reflection of gravity waves are the predominant process in supercritical shear flow.

Pinilla & Chu (2008, 2009a,b) and Chu (2010) have studied numerically the role of gravity-wave radiation on the development of shear flow in shallow open channel. Figure 1 shows their simulations of the shear instabilities of a hyperbolic tangent velocity profile for three different convective Froude numbers: (a) $Fr_c = 0.4$, (b) $Fr_c = 0.8$ and (c) $Fr_c = 1.2$. The columns on the left-hand side of the figure show the velocity vectors and the columns on the right-hand side show the dilation. The evolution of a small disturbance with time eventually leads to large scale lateral exchanges between the two sides of the shear flow of different velocities. At low convective Froude number when $Fr_c = 0.4$, the mass and momentum exchanges as shown in Fig. 1(a) are characterized by the formation of the turbulent eddies. At high convective Froude number when $Fr_c = 1.2$ as shown in Fig. 1(c), the exchanges are characterized by the radiation of gravity wave and the less energetic sliding shocklets. Radiation of gravity waves from the shocklets has reduced the instability and suppressed the mass exchanges across the shear layer.

Similar dependence of the shear instability on the convective Froude number is obtained from the linear stability analysis using the normal mode approach as shown in Fig. 2. For the hyperbolic-tangent base velocity profile, the exponential growth rate α_{max} decreases with the convective Froude number Fr_c. This dependence on the convective Froude number for the shear flow in open channels is analogous to the shear instability of compressible gas dynamics. The lines for Mach number Ma = 0.01, 0.4, 0.8 and 1.2 in Fig. 2 are instability calculations obtained for ideal gas by Sandham & Reynolds (1990). The gravity-wave radiation from the shear flows in open channels has the similar effect on instability as the radiation of the sound from the shear layer in compressible gas.

Figure 3 shows another shear-flow exchange between an open-channel flow with an array of side basins for two different Froude numbers: Fr_c

= 0.35 and 1.6. The subcritical-flow exchanges with Fr_c = 0.35 are characterized by the development of eddies while the supercritical flow with Fr = 1.6 is predominated by the radiation of the gravity waves.

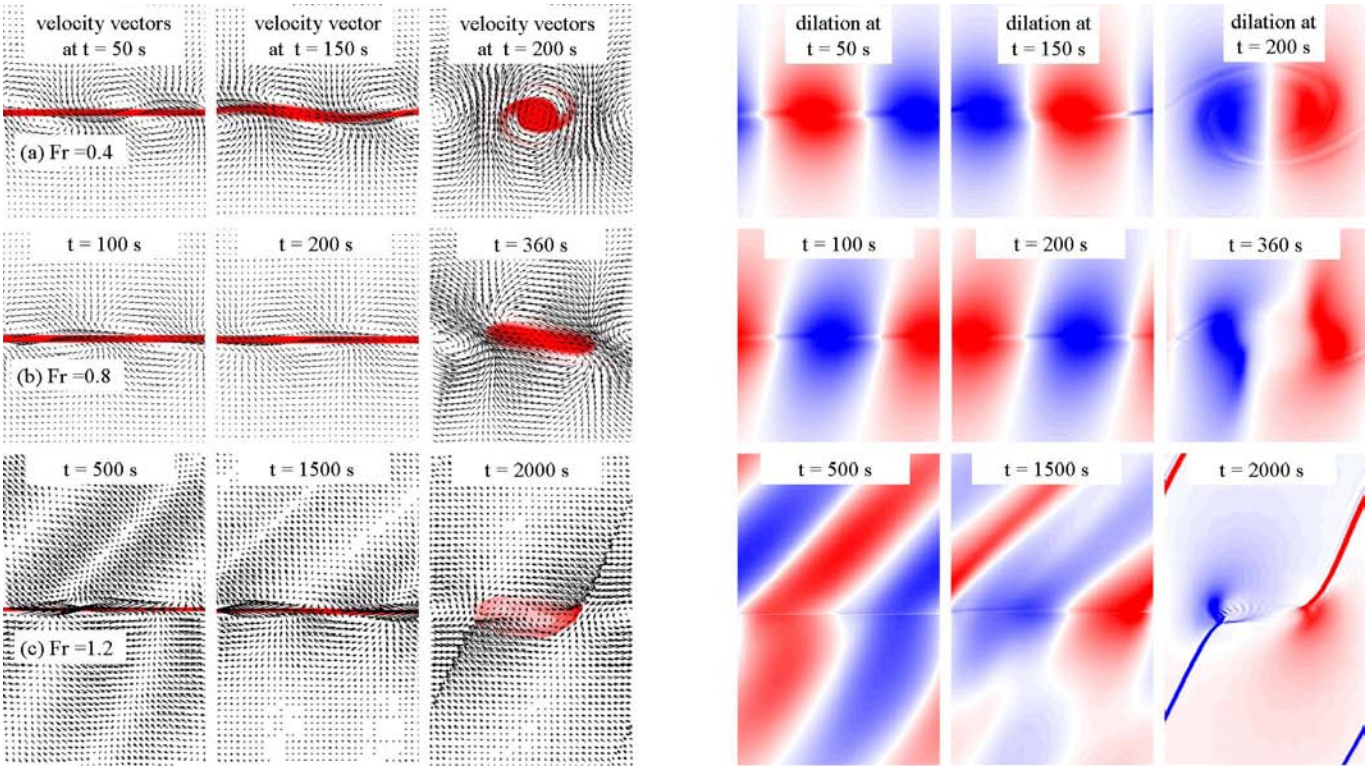

Figure 1 Development of shallow shear flow of hyperbolic-tangent velocity profile for three convective Froude numbers; (a) Fr = 0.4, (b) Fr = 0.8 and (c) Fr = 1.2. The three left-hand columns show the velocity vectors and the rollup of a thin layer of dye between the shear flows moving in opposite directions. The three right-hand columns show the dilation of the depth-averaged velocity. Radiation of gravity waves characterizes the shear flow of large convective Froude number Fr = 1.2 in (c).

2 EXPERIMENT

To study the role of the gravity waves on the shear instability, laboratory experiments were carried out for the mass exchanges between an open-channel main flow and an array of side basins. Figure 4 shows the arrangement of the experiment in the laboratory. An array of basins is attached along the side of the main open-channel flow in a 8.84-m long and 1.41-m wide tilting flume. The side basins are open to the main channel flow to allow the flow exchanges with the main flow. The basins are square in shape. The dimensions of the basins are K =15 cm in one series of experiment K = 45 cm in the other. The basins along side of the open channel are the macro roughness in a conceptual model of the river flow.

During the experiments, red dye of concentration c_o was introduced to the upstream edge of the first basin as the tracer at a rate q_o for a period of time until the dye concentration in the basin reached a quasi-steady state. The measurement of the dye concentration in the basin was based on a video imaging method developed by Zhang & Chu (2003). Since the green light was reduced by the presence of the red dye, the dye concentration was correlated with light absorption by the dye. The accumulation and the retention of the dye in the basins are determined for the flows of a range of Froude numbers from

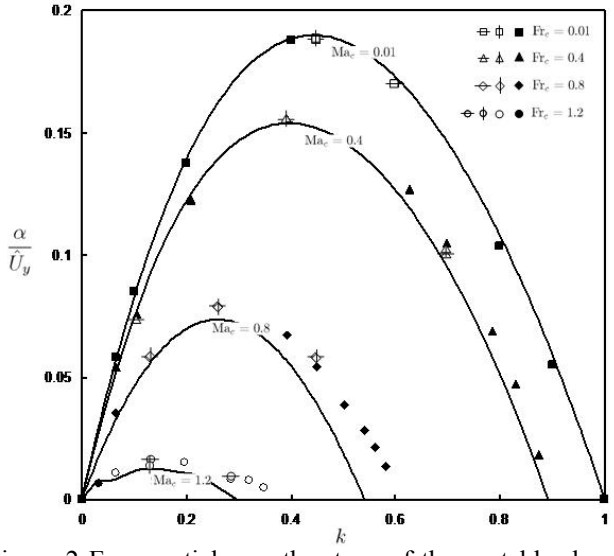

Figure 2 Exponential growth rate α of the unstable shear flow of the classical hyperbolic tangent velocity profile. Its dependence on the convective Froude number Fr_c is analogous to the dependence of the rate α on the Mach number Ma in the compressible shear flow.

Fr = 0.26 to 3.5. Overall parameters such as the accumulation time τ_a and the retention time τ_r are determined from the measurements to characterize the lateral exchanges of the dye tracer between the side basins and the main flow in the open channel.

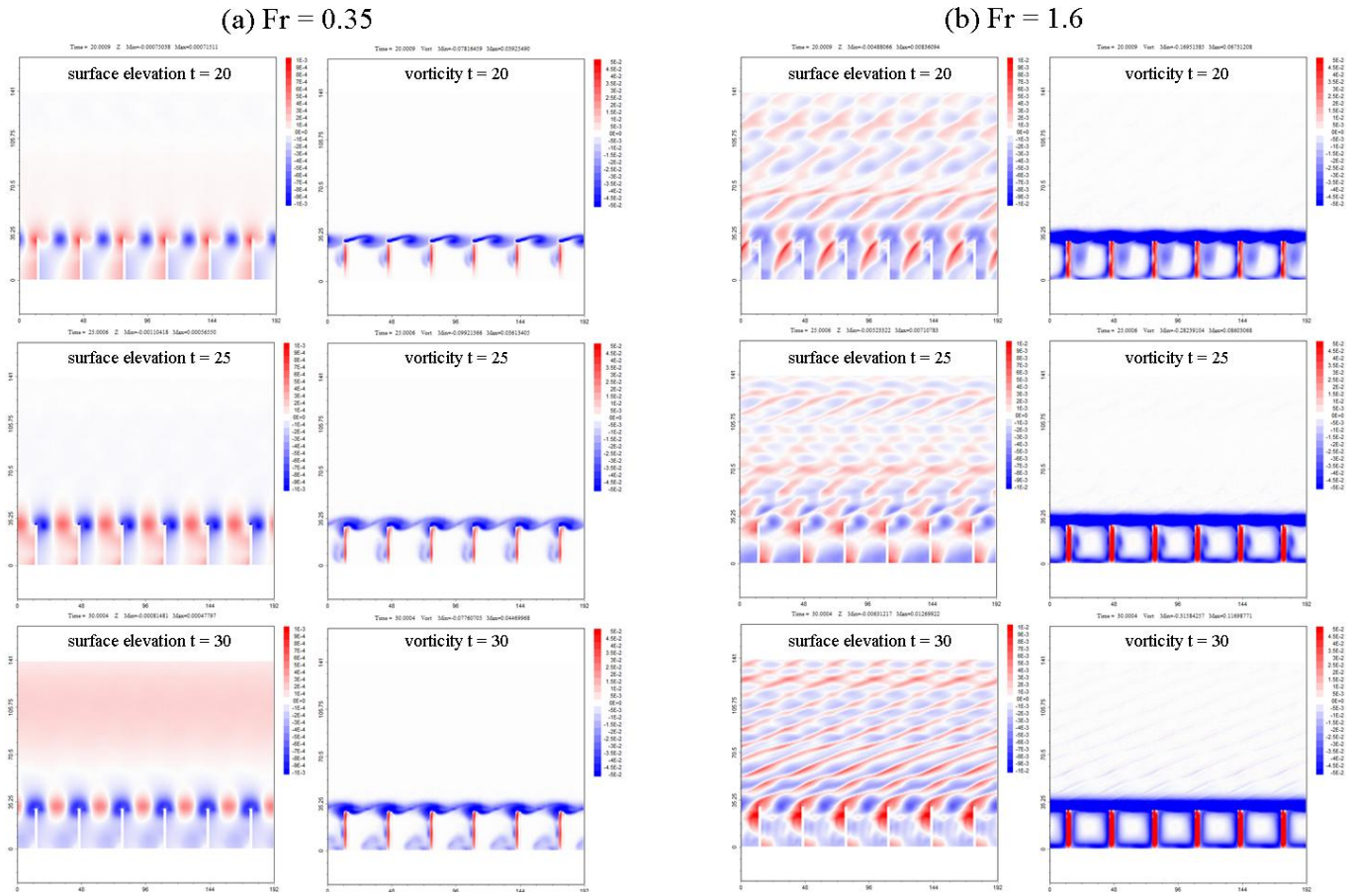

Figure 3 Numerical simulation of the flow exchanges between a main open-channel flow and an array of square basins for two Froude numbers; (a) subcritical flow with Fr = 0.35 and (b) supercritical flow with Fr = 1.6. These numerical computations were carried using a numerical scheme developed by Pinilla et al. (2010).

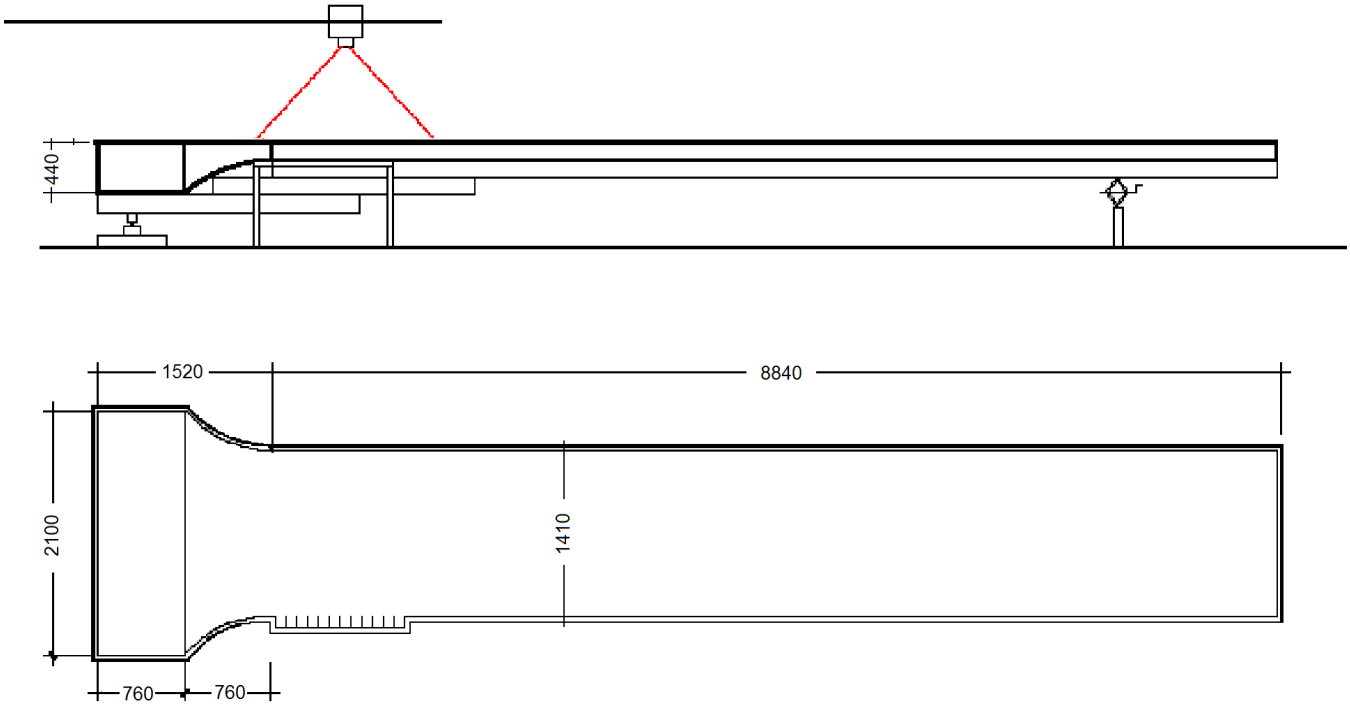

Figure 4 Side view and top view of the tilting flume. An array of 12 square basins is installed along side of the main open-channel flow on a tilting flume.

The tests were conducted for supercritical flow of Froude number Fr = 1.51, 1.52, 1.92, 3.5 and a subcritical flow of Froude number Fr = 0.26 on the channel slopes of S_o = 0.05 and 0.008, respectively. The test conditions including water depth h and velocity U in the main channel were summarized in Table 1.

Table 1. Laboratory experiments conditions

Test no.	channel slope S_o	basin size K (cm)	depth h (cm)	velocity U (m/s)	Fr
1	0.05	15	1.0	1.09	3.50
2	0.008	15	5.0	0.185	0.26
3	0.008	15	1.9	0.651	1.51
4	0.008	15	0.9	0.571	1.92
5	0.008	45	2.1	0.691	1.52

The presence of the red dye in the basin of depth h reduced the intensity of the green light. As shown in Fig. 5, both incident light and reflected light were reduced. The percentage of the green-light intensity reduction p was used to determine the dye concentration. Figure 6 shows the calibration curves for the dye concentration. The concentration c/c_o is related to p by three curves for three different water depths h = 1.5 cm, 3.0 cm and 6.0 cm.

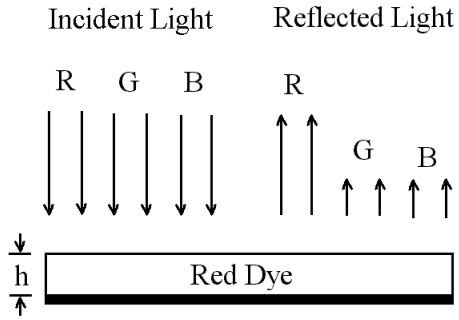

Figure 5 Absorption of green (and blue) light due to the presence of red dye in the open-channel flow of depth h.

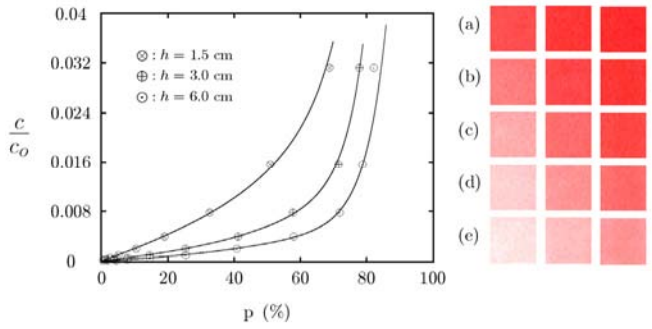

Figure 6 Calibration curves correlating the percentage of the green-light absorption p with the dye concentration c/c_o.

3 EXPERIMENTAL RESULTS

The dye in the basins increased with time. The supply of the dye from the leading edge of the first basin was maintained until the dye concentration in the basins reached a quasi-steady state. The source of the dye supply was then shutoff to allow the dye concentration in the basin to reduce with time. Figure 8 shows the dye-concentration images in the re-circulating region inside the basin after the supply of the dye had been turned on from the upstream source while Fig. 7 shows the retention images after the dye had been shutoff. The images for the subcritical main flow in Fig. 7 are different from the images in Fig. 8 for the supercritical main flow. The entrainment of fresh water from the main flow in the channel is observed by the bright area in the basin where the dye concentration has been reduced. The process of the entrainment was intermittent as the blobs of fluid entered the basin from the main stream and then circulated around the edges of the basin. In subcritical flow (Fig. 7), the entrained fluid blobs

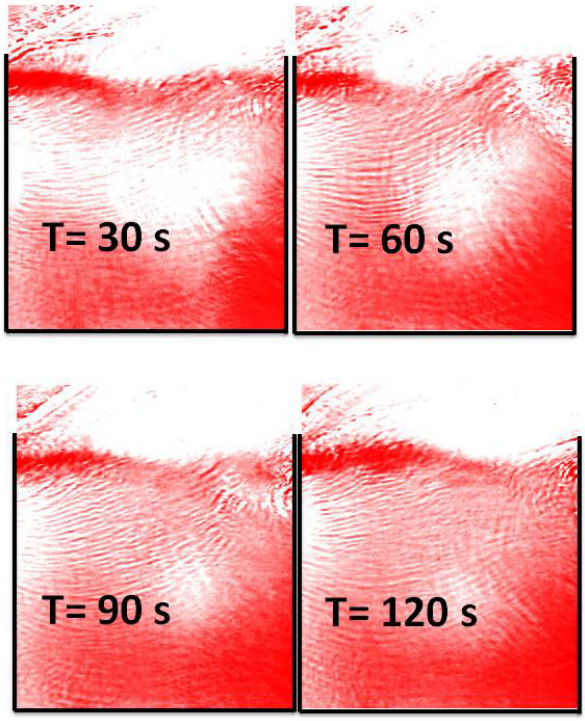

Figure 7 Subcritical flow images of the dye retention in basin no. 1; Fr = 0.26, K=15cm, h =5cm.

were in the shape of eddies. In supercritical flow (Fig. 8), the entrained fluid was not as well defined. Gravity waves were generated as the supercritical main flow interacted with the water in the basin. The radiation of the gravity waves away from the basins was intense but had not produced any positive effects on the entrainment. In comparison with the case of the subcritical main flow,

the shear layer between the supercritical main flow and the flow in the basin was less energetic.

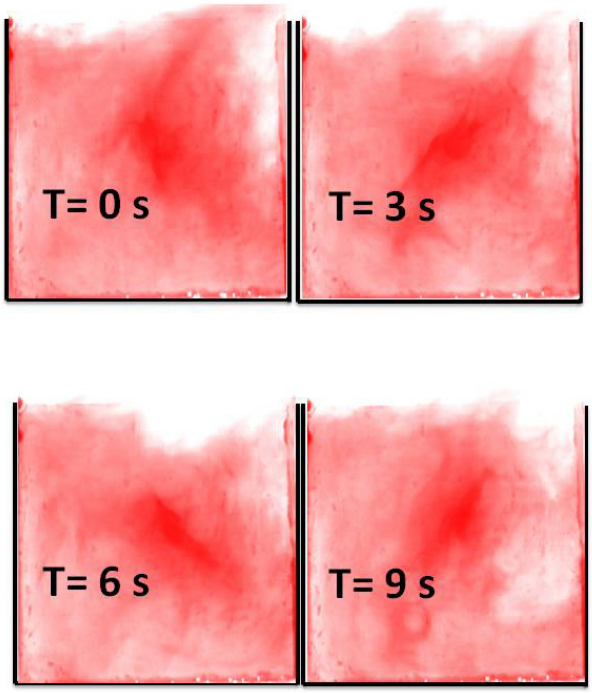

Figure 8 Supercritical flow images of the dye accumulation in basin no. 1; Fr = 1.52, K = 45cm, h = 2.1cm.

The concentrations in the center of basins are plotted in Figs. 9 and 10 versus time. The plots are dimensionless. The dimensionless dye concentration is $c^* = (cUhK)/(c_o q_o)$, which is obtained by the normalization of the source dye mass flux $c_o q_o$. The dimensionless time is $t^* = tU/K$, where U is averaged flow velocity in the main channel and K is the dimension of the square basins. The concentration of the dye in the basins c^* first increased with time t^*. It reaches a quasi-steady state after a period of time. The decay of the dye concentration in the basin is subsequent to the quasi-steady state after the dye supply is shutoff from the upstream source. A curve of the following functional form is fitted through the experimental data for the period during the accumulation phase:

$$c^* = c^*_{qs}[1 - \exp(-\frac{t}{\tau_a})] \quad (1)$$

where τ_a = is the dimensionless accumulation time and c^*_{qs} = is the dimensionless quasi-steady concentration. The reduction of the dye concentration with time for the period during the decaying phase is fitted with the follow function:

$$c^* = c^*_{qs} \exp(-\frac{t}{\tau_r}) \quad (2)$$

where τ_r = is the dimensionless retention time.

The accumulation time scale τ_a and the retention time scale τ_r are the dimensionless parameters that are introduced to characterize the overall exchanges of fluids in the basins with the main flow in the open-channel. A large value of the dimensionless time scales would suggest a slow exchange process and vice versa. Booij (1989) has used the retention time τ_r to define the exchanges of subcritical flow in harbours. Altai & Chu (1997) determined the retention time τ_r for a wider range of the subcrtical Froude numbers, and found the retention time to have comparable values as those obtained by Booij (1989).

The functions defined by Eqs. 1 and 2 fit quite well with the concentration data obtained in the present series of experiments. Table 2 summarizes the values of the dimensionless accumulation and retention time scales from the experimental data obtained in the first basin no.1 and the third basin no.3.

Table 2. Accumulation and retention time scales for different experiments

Test no.	Fr	Basin no.	Accumulation time scale τ_a (s)	Retention time scale τ_r (s)
1	3.50	1	31	150
		3	120	145
2	0.26	1	40	32
		3	50	40
3	1.51	1	125	100
		3	75	85
4	1.92	1	125	150
		3	105	120
5	1.52	1	175	150
		3	75	85

The value of the dimensionless accumulation time is different from one basin to the other basin. The first basin no. 1 tends to have smaller dimensionless accumulation time than the accumulation time scale of the downstream basin no. 3. However, the retention time is more uniform. The dimensionless retention time of the first basin is almost the same as the third basin. It appears that the retention time is a better measure of the mass exchange process between the basin and the main open-channel flow.

The values of the retention time for the subcritical main flow are rather reasonable. It is comparable in magnitude to the previous results obtained by Booij (1989) and Altai & Chu (1997) for similar shear flows. However, the dimensionless retention time for the case of the supercritical main flow is three to four times greater than the value for the subcritical flow case.

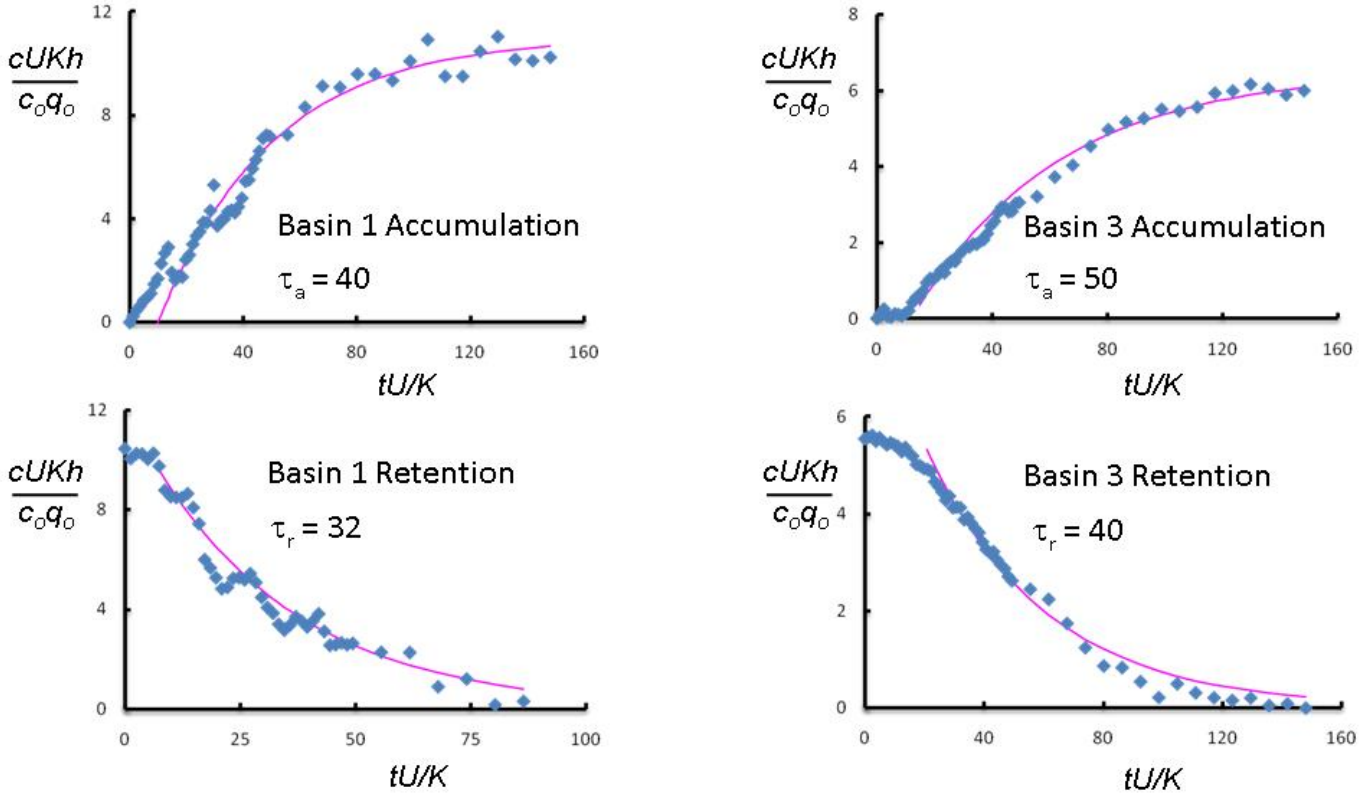

Figure 9 Accumulation and retention of the dye in basin 1 and the basin 3 for a subcritical main flow. The circle symbol denotes the experimental data. The lines are Eqs. 1 and 2 that best fit the data.

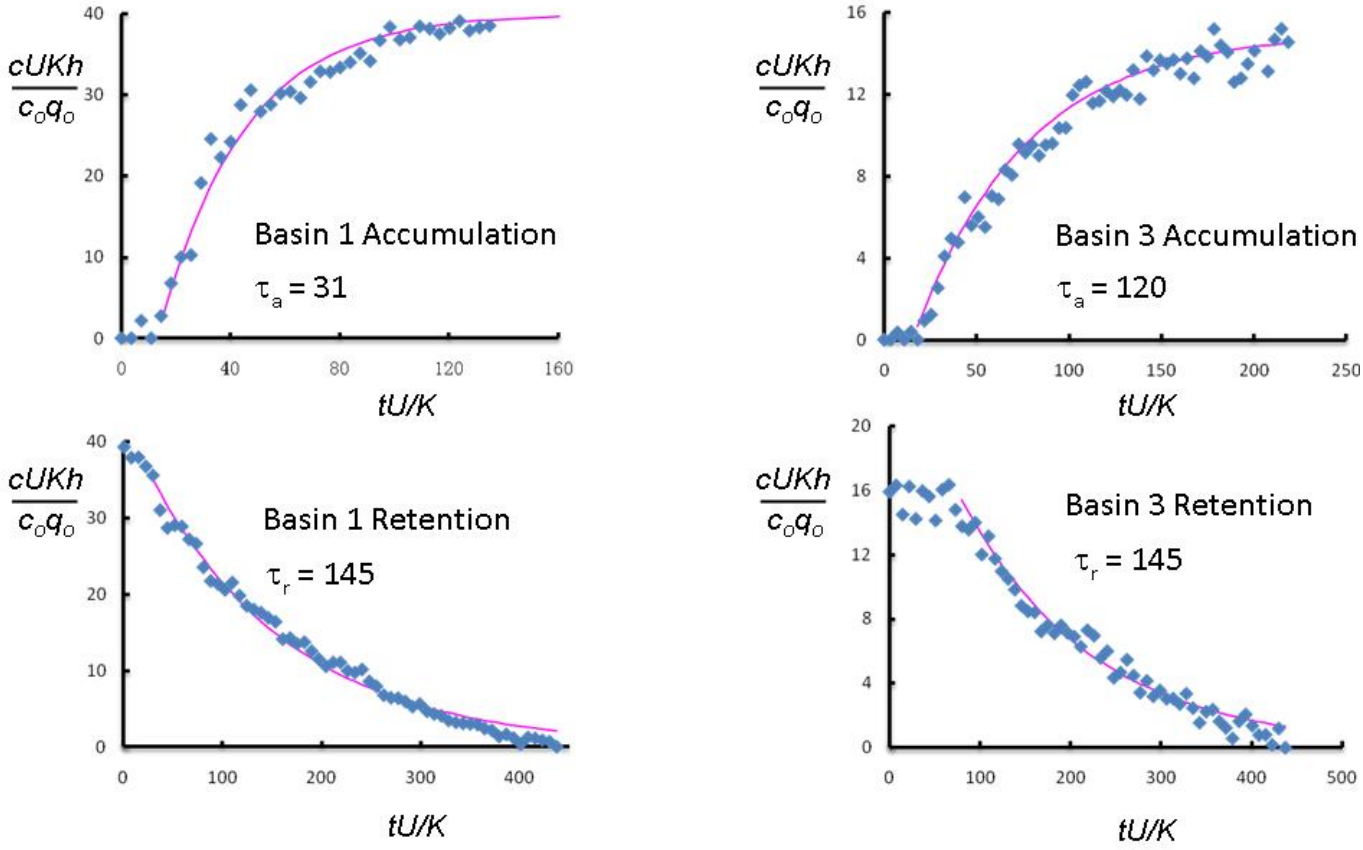

Figure 10 Accumulation and retention of the dye in basin 1 and the basin 3 for a supercritical main flow. The circle symbol denotes the experimental data. The lines are Eqs. 1 and 2 that best fit the data.

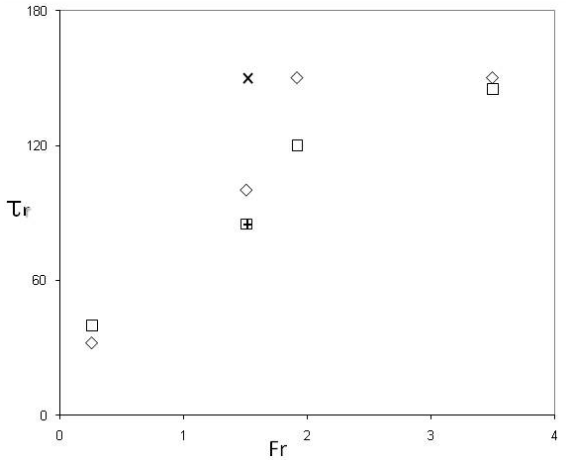

Figure 11 Retention time versus Froude Number of the dye in basin 1 and basin 3 (◇: Basin 1 K = 15cm, □: Basin 3 K = 15cm, ×: Basin 1 K = 45cm, +: Basin 3 K = 45cm.)

Figure 11 plots the retention time τ_r versus the Froude number Fr obtained from the present series of experiments. The retention time is about τ_r = 40 for subcritical flow of small Froude number and is as high as τ_r = 150 for supercritical flow of large Froude number. It is clear that the mass exchange processes in the supercritical flow are different from the processes in subcritical flow. The exchanges in the subcritical flow are characterized by the rollup of the fluid in the coherent eddies and the excitation of the shear layer by the gravity-wave feedback as evident in the dyed flow images shown in Fig. 7. On the other hand, the exchanges in the supercritical flow are due to gravity-waves radiation from the shear layer in a manner analogous to the development of supersonic shear layers in compressible fluid (Bogdanoff 1983, Papamoschou & Roshko 1986, Kim 1990). There were no evidence that can be found in Fig. 8 to suggest that the coherent eddies had formed in the supercritical shear layer. Although significant flow oscillations were produced by the radiation of the gravity waves, the presence of the gravity waves did not seem to have any direct effect on the mass exchanges of the dye between the basins and the supercritical main flow. The indirect effect of wave radiation on the shear instability is however expected.

4 CONCLUSION

The retention and accumulation times are overall parameters that characterize the mass exchanges across the flow between the main channel and its side basins. The measurement of these parameters using the video imaging technique has supported the conclusion obtained from hydrodynamic stability analysis that the supercritical shear layer is more stable to disturbance and as a consequence less energetic for the exchanges of mass across the shear layer.

The transverse exchanges of the mass in the subcritical open-channel flow are relatively understood. Much is still to be studied of the process in the supercritical shear flow. The retention and accumulation time are the parameters only for the overall exchanges. Turbulence measurements in the supercritical shear flow are to be conducted for better understanding of the process.

REFERENCES

Alavian, V. and Chu, V. H. (1985) "Turbulent exchange flow in shallow compound channel," Proceedings of 21st Congress of IAHR, pp. 446-451.

Altai, W. and Chu, V. H. (1997) "Rentention time of a recirculating flow," Proc. 27th IAHR Congress, San Francisco, Theme B, Vol. 1, Theme B, pp. 9-14.

Altai, W., Pinilla, C. and Chu, V.H. (2005) "Shallow recirculating flow in a cavity," in Environmental Hydraulics and sustainable Water Management, Lee & Lam (eds) Taylor & Francis Group, London (ISBN 04 1536 546 5), pp. 995-1000.

Bogdanoff, G.A. (1983) "Compressible effects in turbulent shear layers," AIAA Journal, Vol. 21, pp. 026-927.

Booij, R. 1989. "Exchange of mass in harbours. Proc. 23rd IAHR Congress, Vol. D, 69-74.

Chu, V.H. (2010) "Shear instability, wave and turbulence simulations using the shallow water equations," J. Hydro-Environ. Res., Vol. 4, part 2, pp. 173-178.

Knight, D.W. and Shiono, K. (1990) "Turbulent measurements in a shear layer region of a compound channel," J. Hydrualic Research, Vol. 28, pp. 175-196.

Kim, S.C. (1990) New mixing length model for supersonic mixing layer, AIAA Journal," Vol. 28, pp. 1999-2000.

Lambert, M.P. and Sellin, R.H.J. (1996) "Discharge prediction in straight compound channels using the mixing length concept," J. Hydrulic Research, Vol. 34, pp. 381-394.

Papamoschou, D. And Roshko, A. (1986) "Observation of supersonic free shear layer," AIAA paper 86-0162.

Pinilla, C., Bouhairie, S., Tan, L.W. and Chu, V.H. (2010) "Minimal intervention to simulations using the shallow-water equation," J. Hydro-Environ. Res., pp. 201-207.

Pinilla, C. and Chu, V.H. (2008) "Waves and Bed-Friction Effect on Stability of Transverse Sheer Flow in Shallow Waters," Journal of Coastal Research, Vol. S52, ISSN 0749-0208, pp. 207-214.

Pinilla, C.E. and Chu, V.H. (2009a) "The Role of Wave Radiation on Instability of Coastal Current," Proc. 33rd Congress of IAHR, ISBN 978-90-78046-08-0, Aug 9-14, Vancouver, Canada, 8 pp. in CD ROM.

Pinilla, C.E. and Chu, V.H. (2009b) "Wave radiation and shear instability in rotating stratified flow," Proc. 28th Int. Conf. on Ocean, Offshore, and Arctic Eng., ISBN 978-0-7918-3844-0, May 31- June 5, Honolulu, Hawaii, ASME paper OMAE2009-79416, 8 pp.

Sandham, N.D. and Reynolds, W.C. (1990) "Compressible mixing layer: Linear theory and direct numerical simulation," AIAA Journal, Vol. 28, pp. 618-624.

Tamai, N., Aseada, T. and Ikeda, H. (1986) "Study on generation of periodical large surface eddies in a composite channel flow," Water Resource Res., Vol. 22, pp. 1129-1138.

Van Prooijen, B.C., Battjes, J.A. and Uijttewaal, W.S.J. (2005) "Momentum exchange in straight uniform compound channel flow," J. Hydraulic Engineering, Vol. 131, pp. 175-183.
Zhang, J.-B. and Chu, V.H. (2003) "Shallow turbulent flows by video imaging method," J. Engineering Mechanics, ASCE, Vol. 129, pp.1164-1172.